ADVANCED FUNCTIONAL MATERIALS
www.afm-journal.de

Emulsifier-Free Graphene Dispersions with High Graphene Content for Printed Electronics and Freestanding Graphene Films

*Folke Johannes Tölle, Martin Fabritius, and Rolf Mülhaupt**

A novel and highly versatile synthetic route for the production of functionalized graphene dispersions in water, acetone, and isopropanol (IPA), which exhibit long-term stability and are easy to scale up, is reported. Both graphene functionalization (wherein the oxygen content can be varied from 4 to 16 wt%) and dispersion are achieved by the thermal reduction of graphite oxide, followed by a high-pressure homogenization (HPH) process. For the first time, binders, dispersing agents, and reducing agents are not required to produce either dilute or highly concentrated dispersions of single graphene sheets with a graphene content of up to 15 g L^{-1}. High graphene content is essential for the successful printing of graphene dispersions by 3D microextrusion. Free-standing graphene films and micropatterned graphene materials are successfully prepared using this method. Due to the absence of toxic reducing agents, the graphene exhibits no cytotoxicity and is biocompatible. Furthermore, the electrical conductivity of graphene is significantly improved by the absence of binders. Flexible microarrays can be printed on different substrates, producing microarrays that are mechanically stable and can be bent several times without affecting electrical conductivity.

1. Introduction

Graphene is an atom-thick carbon sheet with a honeycomb-like arrangement of sp^2-hybridized carbon atoms in a single layer.[1] The 2D polycyclic aromatic carbon macromolecule exhibits a unique combination of high electrical and thermal conductivity, high stiffness, tear and abrasion resistance, chemical and thermal stability, gas barrier performance, and absorption of UV and IR radiation.[2–5] For many applications, especially those related to printing processes, it is desirable to have the ability to disperse graphene in different media. The incorporation of functional groups during graphene synthesis can render functionalized graphene (FG) amphiphilic and enables the electrostatic and steric stabilization of graphene[6,7] as well as its interfacial coupling with various materials, including polymers.[8] FG with variable functional group content is easily obtained using a two-step process. After the oxidation of graphite to graphite oxide (GO), the reduction can be performed by either a chemical reducing agent, producing chemically reduced graphite oxide (CRGO), or the rapid thermolysis of GO at temperatures exceeding 400 °C, producing thermally reduced graphite oxide (TRGO).[9–15]

In contrast to the graphene obtained by graphite peeling or epitaxial growth, FG has a wrinkled architecture that contains functional groups such as hydroxyl, phenolic, and carboxyl groups.[16,17] Despite the presence of structural defects and functional groups, FG exhibits a high Young's modulus and electrical conductivity, whereas its thermal conductivity is low.[2,18,19] The dispersion of graphene is an important prerequisite for the development of solvent-based large-scale FG processing, including surface coatings, graphene films, carbon paper, and conducting surface patterns for applications in flexible electronics, displays, electrodes, and sensors.

Because GO is easy to disperse in water, aqueous GO inks have been successfully used in the inkjet printing of GO films and patterns.[20,21] However, a post-treatment step is required to convert the non-conducting GO into conducting FG nanosheets by chemical reduction. This conversion can be achieved by the exposure of GO to hydrazine vapors or by a heat treatment.[20–22] Unfortunately, these processes limit the scope of FG materials to those that are stable at high temperatures and prepared on chemically inert substrates. It would be significantly more convenient to process FG dispersions directly and omit any post-treatment steps.

At present, three strategies exist for the production of FG dispersions from GO without post-treatment: i) reduction of aqueous GO dispersions in the presence of surfactants or binders that emulsify FG;[16,23–26] ii) organic modification of GO, TRGO or CRGO to enable dispersion in aqueous and non-aqueous media;[27–31] and iii) formation of an emulsifier-free dispersion of CRGO that is restricted to very low graphene content (<0.25 g L^{-1}).[6,32] For most applications, it is imperative to eliminate the use of toxic reducing agents, such as hydrazine, that produce large amounts of byproducts

F. J. Tölle, M. Fabritius, Prof. R. Mülhaupt
Freiburg Materials Research Center (FMF)
Freiburg Institute for Advanced Studies (FRIAS),
and Institute for Macromolecular Chemistry of the
Albert-Ludwigs University Freiburg
Stefan-Meier-Str. 31, D-79104 Freiburg, Germany
E-mail: rolf.muelhaupt@makro.uni-freiburg.de

DOI: 10.1002/adfm.201102888

and require an additional purification post-treatment. Furthermore, binders and emulsifiers introduce impurities that impair electronic properties. Therefore, a new approach for the clean and facile large-scale production of FG dispersions is in high demand. Because conventional methods such as prolonged sonication fail to produce stable FG dispersions via the disagglomeration of stacked graphene sheets, we attempted to find a more thorough method. High-pressure homogenization (HPH) is a particularly interesting procedure due to the high sheer forces involved, which should allow for disagglomeration. Additionally, the excellent control provided by this process can prevent the complete destruction of the graphene sheets. Herein, we present for the first time a versatile new process for the preparation of aqueous and non-aqueous emulsifier- and binder-free graphene dispersions with FG contents of up to 15 g L^{-1}, which do not require any pre- or post-treatment.

To demonstrate the versatile applications of these new dispersions, we used them in the formation of freestanding graphene films and in a printing process based on microextrusion. For example, freestanding graphene films and papers can be used for the fabrication of lightweight anodes for lithium-ion batteries.[33,34] In contrast to carbon paper made from GO, the FG-based carbon paper derived from aqueous FG dispersions and pastes is electrically conductive.[35,36] To date, several routes have been explored for the fabrication of graphene paper, including the direct exfoliation of graphite in the presence of surfactants,[26] chemical reduction of a GO dispersion followed by filtration using hydrazine as a reducing agent[37] and post-reduction of GO films, requiring either a reducing agent or thermal post-treatment.[33,38,39]

Graphene sheets and papers offer attractive opportunities for biomedical applications. At present, it is widely accepted that graphene films are biocompatible.[37,40] Therefore, it is crucial to exclude any cytotoxic impurities (e.g., hydrazine), which are mainly present in the CRGO. Recent studies evaluated the use of graphene for drug delivery devices,[41] stem cell research,[42,43] and tumor therapy.[44] In vitro experiments have demonstrated graphene's potential as a tissue culture material for neural systems.[45] As neural cells are electroactive and communicate by electric signaling, the electrical properties of graphene, together with its biocompatibility, make it particularly interesting for nerve repair or even the design of neural chips. Accordingly, we performed cell culture experiments to assess the biocompatibility of FG films.

Printing FG using inkjet printing without post-treatment has been reported by Dua, Ruoff, and co-workers, who employed CRGO-based FG dispersions to print vapor sensors.[24] Their graphene ink-forming process includes the chemical reduction of GO and the subsequent dispersion of CRGO using a non-ionic surfactant. Other research groups have used a wide variety of organic and inorganic binders together with ionic and non-ionic surfactants to obtain FG-based printing inks.[23,25] Although emulsifier-containing conducting graphene printing inks and suspensions are commercially available, e.g., Vor-ink from Vorbeck, their formulations have not been disclosed.[46] Other reports have described the direct printing of graphene dispersions (PureSheets, Nanointegris) containing noble-metal nanoparticles.[47] To date, high costs and low graphene contents limit the application of such dispersions.[48] To further improve FG processing by a printing technique, viscous pastes of conducting FG are employed in a novel 3D dispensing process to print conducting graphene micropatterns and fabricate conducting graphene films. The ability to print defined patterns is of major interest for biomedical device design and fabrication. In this paper, we demonstrate the unique structure-property investigations afforded by excellent control over FG synthesis, a superior dispersion technique and innovative processing methods.

2. Results

2.1. Emulsifier-Free Dispersion of TRGO

As mentioned in the previous section, there are currently two key problems in graphene production and dispersion. The first problem lies in the production process and can be described as a compromise between the small-scale production of pristine graphene and the large-scale production of FG that often contains impurities caused by the chemical processes involved. The second problem is the poor dispersability of graphene, which either results in dispersions with very low graphene content or requires the use of surfactants or binders, which in turn results in the deterioration of graphene's attractive physical properties. Herein, we present a way to address both problems with a two-step process that allows a clean, large-scale production of stable FG dispersions without the use of additives.

As outlined in **Scheme 1**, TRGO is synthesized via the oxidation of graphite to GO (Hummer's method),[9] which is reduced

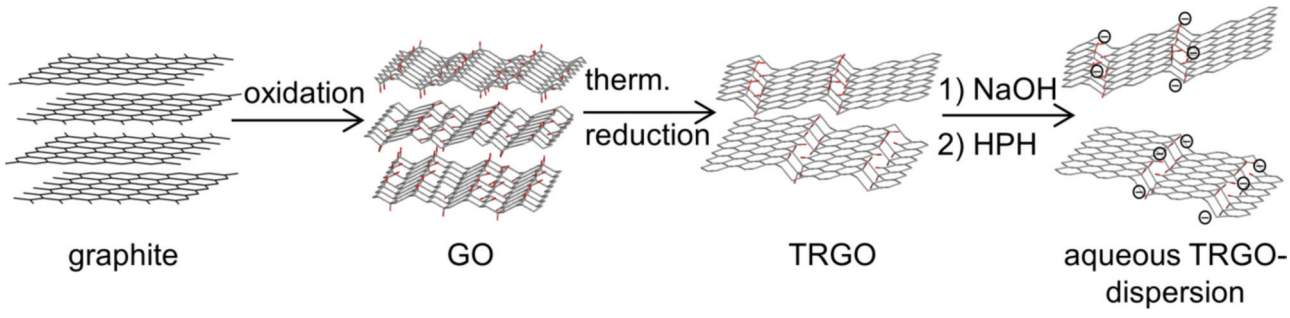

Scheme 1. Preparation of emulsifier-free aqueous TRGO dispersions: graphite is oxidized and forms GO, which generates TRGO upon thermal reduction. Upon the HPH treatment of TRGO, anionic graphene sheets are dispersed in an alkaline medium.

by rapid heating above 400 °C. This process yields a fine TRGO powder without requiring a chemical reducing agent. However, the dispersability problem remains. Some reports suggest the possibility of creating stable aqueous dispersions of CRGO.[6,32] Nevertheless, CRGO-based graphene dispersion methods require tedious purification due to a large byproduct formation caused by both the oxidation of graphite and the subsequent oxidation of the reducing agents. In the case of hydrazine addition, ammonium salts are formed in the CRGO process, and the resulting CRGO sheets contain nitrogen functionalities.

With regard to TRGO, all conventional methods fail to disperse single nitrogen-free graphene sheets in water in the absence of surfactants and binders. Even after prolonged sonication, no stable dispersions are obtained, and significant sedimentation occurs (cf. photograph in **Figure 1**a). Large particles composed of graphene stacks are visible in the transmission electron microscopy (TEM) images shown in Figure 1c.

This work addresses this problem using a high-pressure homogenizer. In this device, the TRGO dispersion is forced through a narrow gap of the homogenizing valve under high pressure to form stable FG dispersions (Figure 1b). At pressures of up to 1500 bar, high shear forces and turbulences, together with compression, acceleration, pressure drop, and impact, result in an effective disintegration of TRGO to produce stable dispersions of much smaller particles. As can be seen in the TEM images in Figure 1d, the TRGO dispersion is effective and produces single FG sheets that are uniformly dispersed in water. The dispersions appear homogeneous to the naked eye even after several months of storage. Over time, a minor black residue forms at the bottom of each flask. This residue can easily be redispersed by sonication or simple shaking or be removed by centrifugation.

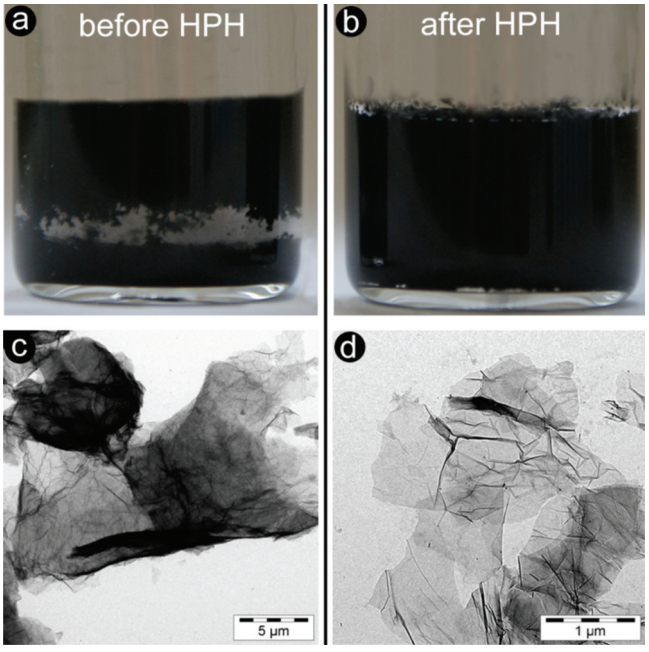

Figure 1. a,b) Photographs and c,d) TEM images of TRGO dispersions in water at pH 9–10. The dispersions were produced by sonication (a,c) and subsequent HPH process (b,d).

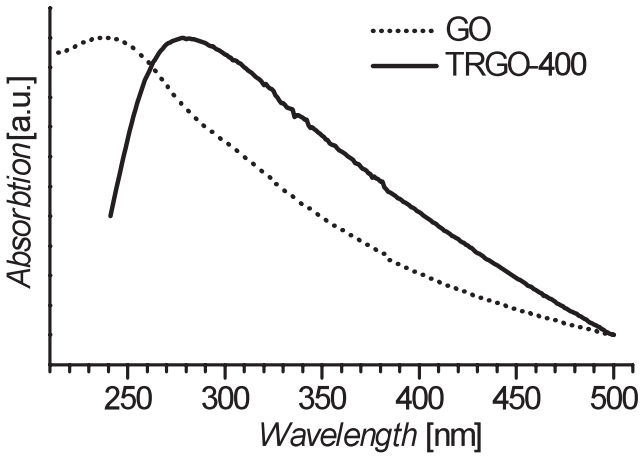

Figure 2. UV–vis spectra of aqueous GO (maximum at 237 nm) and TRGO-400 (maximum at 279 nm) (0.03 g L^{-1}, background-corrected and normalized).

In contrast to the previously mentioned CRGO-based dispersions, TRGO-based dispersions obtained by the HPH process are free of nitrogen, ammonium cations and other residues typically associated with a chemical reduction. Furthermore, the HPH process enables the production of stable TRGO dispersions in both water and organic solvents such as acetone and isopropanol (IPA). This feature is of interest because it allows the FG sheets to be transferred into a variety of organic media, including monomers.

The most prominent feature of the HPH process is the facile production of FG dispersions and pastes with a wide range of graphene incorporations all of which form stable dispersions. Currently, a maximum concentration of 15 g L^{-1} of graphene in water has been achieved, which results in a highly viscous graphene paste suitable for the layer-by-layer printing processes described later in this paper. The TRGO-based dispersions with lower concentrations of 0.03 g L^{-1} can be characterized using UV–vis spectroscopy (**Figure 2**). The spectra show broad signals with maxima at 237 nm (GO) and 279 nm (TRGO). These peaks are attributed to the π–π* transitions of the aromatic C=C bonds. The redshift observed upon the reduction of GO to TRGO reflects the restoration of the aromatic system and could be used to monitor the degree of reduction.[6,32,49] The maximum peak of 279 nm for TRGO is significantly higher than the values reported for CRGO prepared by hydrazine reduction (268–270 nm).[6,32] This difference might indicate that a higher degree of reduction is achieved by thermal processes above 400 °C.

As demonstrated, the HPH process is a versatile route for creating stable graphene dispersions. These dispersions can be used for a wide range of applications, including surface-coating and printing on temperature-sensitive substrates such as paper and polymer foil (see Section 2.3). As the thermal reduction step is conducted before the dispersion step, this procedure does not require additional thermal or chemical post-treatment.

2.1.1. Effects of Oxygen Content and Solvent Choice on the Stability of TRGO Dispersions

The stability of TRGO dispersions is influenced by two main criteria: i) the polarity of the solvent and ii) the degree of

functionalization. In the most polar solvent investigated in this study, water, no stable dispersions are obtained unless the reagglomeration and stacking of FG sheets was prevented by electrostatic stabilization. Therefore, we usually perform HPH in a slightly alkaline medium (Scheme 1). The addition of aqueous NaOH (pH 9–10) causes the deprotonation of functional groups in TRGO, such as phenolic and carboxylate groups, and thus renders the FG sheets anionic. The repulsion of anionic FG sheets can account for the significantly improved electrostatic stabilization. A similar stabilization has been reported by Li et al. for CRGO dispersions prepared by the chemical reduction of GO in an alkaline medium.[6] Due to effective electrostatic stabilization, no binders or surfactants are needed.

Upon rapid acidification, the electrostatic stabilization of aqueous dispersions is lost and an uncontrolled flocculation occurs, resulting in uncontrolled stacking. This phenomenon affirms that the electrostatic stabilization is crucial to the stability of aqueous dispersions. Furthermore, this finding might be used to reassemble the FG sheets in a controlled manner by careful protonation and cation exchange to form FG stacks and multilayer graphene assemblies.

Although essential for aqueous dispersions, electrostatic stabilization is not necessary when less polar solvents, such as acetone or IPA, are used. In these solvents, no additives or bases are required and the HPH process yields TRGO dispersions that are stable without electrostatic stabilization. This behavior is attributed to a more favorable interaction between the solvent and the solid, which is caused by the lower polarity of the solvent relative to water.

The second important criterion, the degree of functionalization, is affected by the oxygen content of the TRGO. This value can be controlled by modifying the reduction temperature at which GO is converted into TRGO (**Figure 3**a). The sample code describes the nature of the material and the reduction temperature used (e.g., TRGO-400 denotes the TRGO prepared by thermolysis at 400 °C). The carbon content was measured by elemental analysis (EA), and the oxygen content was calculated from the EA results (**Table 1**). The oxygen content decreases and the carbon content increases with increasing reduction temperature. This finding is in accord with previous reports.[12]

Upon heating, the functional groups decompose and gases such as CO, CO_2, and H_2O evolve.[50] Because the presence of functional groups is crucial for achieving an interaction between the TRGO and the solvent, a minimum oxygen content that corresponds to a maximum reduction temperature is expected. Indeed, we have identified the critical oxygen content for enabling stable aqueous graphene dispersions as >10 wt% O, which is obtained by the reduction of GO at <800 °C. At lower oxygen contents and higher reduction temperatures, flocculation occurs, as evidenced by the significant sedimentation of the aqueous TRGO-800 (0.25 mg mL^{-1}) suspensions. However, the slightly grayish color of the supernatant aqueous phase, together with the pronounced Tyndall effect, indicates that some graphene is still dispersed in water (Figure 3b). Even at a reduction temperature of 900 °C, the Tyndall effect of the supernatant aqueous phase is still observable (Figure 3e). In contrast, the supernatant water phase of suspended TRGO-1000 is clear and does not show any Tyndall effect. As a consequence, attempts to disperse TRGO-1000 (4 wt% O content) in water failed to produce any measureable amounts of dispersed graphene. These findings confirm that low oxygen content (e.g., 4 wt% for TRGO-1000) may not be sufficient to provide electrostatic stabilization of all of the FG sheets.

When acetone or IPA are used as solvents, stable dispersions of TRGO can be produced at 800 °C or 900 °C, respectively (Figure 3c,d). In contrast to the aqueous dispersion medium, the maximum reduction temperature in non-aqueous media is >900 °C with an oxygen content of <6 wt%. These results demonstrate that non-aqueous dispersions of graphene can be produced by the HPH process without the use of any additives, which is attractive for the fabrication of 2D and 3D carbon materials with improved electrical conductivity.

2.2. Freestanding Graphene Paper

The most commonly used procedure for forming freestanding graphene or GO papers is the arrangement of suspended flakes in the flow direction using vacuum filtration, followed by peeling off the filter.[33–35,37] To date, the absence of clean and easy-to-produce suspensions has limited the direct formation of TRGO papers to this process. Consequently, we employed the TRGO dispersions obtained from the HPH process to fabricate freestanding TRGO papers, which are highly flexible and

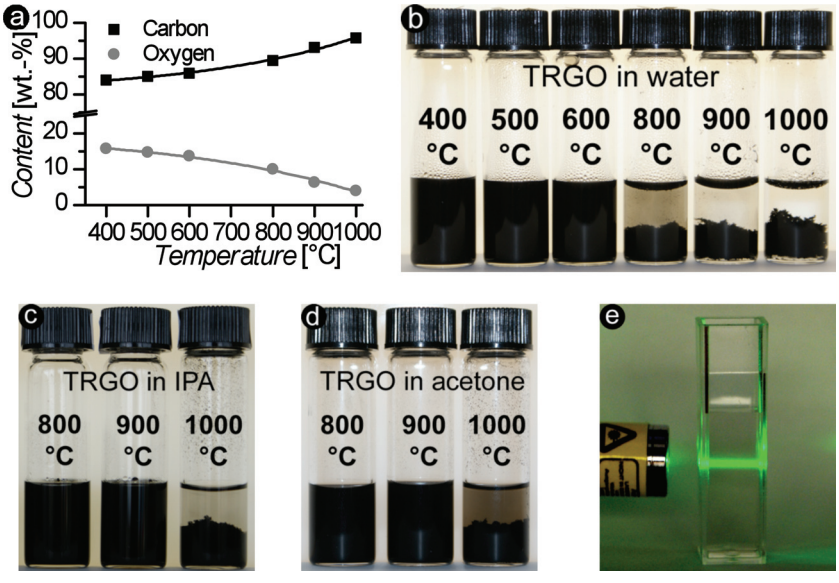

Figure 3. Effect of the reduction temperature on a) the carbon and oxygen content of TRGO, b) the stability of aqueous TRGO dispersions at pH 9-10, and the stability of dispersions in IPA (c) and acetone (d). All dispersions contain 0.25 g L^{-1} FG. In (e), the Tyndall effect of the transparent supernatant aqueous phase of sedimented TRGO-900 suspensions is shown.

Table 1. Elemental analysis of the GO and TRGO samples used in this study.

Sample name	Reduction temperature [°C]	C [wt%]	H [wt%]	O[a)] [wt%]
GO	–	57.7	2.4	39.9
TRGO-400	400	84.0	0.3	15.7
TRGO-500	500	85.0	0.3	14.8
TRGO-600	600	85.9	0.4	13.7
TRGO-800	800	89.5	0.6	10.0
TRGO-900	900	93.1	0.6	6.3
TRGO-1000	1000	95.7	0.3	4.0

No S or N content was detected by elemental analysis.
[a)]Calculated by subtracting the C and H values from 100%.

electrically conductive (**Figure 4**a). The thickness of these papers can be varied from 8 to 22 µm and is controlled by the amount of TRGO used in the process. The conductivity of these thin films was measured using a four-point probe as 10–16 S cm^{-1}.

To demonstrate the thermal stability of the TRGO paper, a "graphene light bulb" was assembled using a strip of TRGO paper as the glow filament (Figure 4b). Although intended as a "fun" experiment (there is no obvious application for this type of light bulb), this finding nevertheless demonstrates the possibility of employing FG dispersions for the fabrication of a carbon-based temperature-resistant electrode material. As mentioned in the introduction, graphene films are considered biocompatible.[37,40] Therefore, removing or avoiding any cytotoxic impurities in the material is essential. To evaluate future applications of graphene papers, such as for highly flexible and biocompatible electrodes, biocompatibility tests were performed.

In the biocompatibility tests of TRGO papers, human osteosarcoma cells (CAL 72) were cultured on top of the TRGO paper (**Figure 5**a,c). Pressed pristine graphite tablets serve as a reference and were likewise cultured (Figure 5b,d). PI/FDA stainings show good cell viability proliferation on both TRGO paper (Figure 5a) and the graphite tablet (Figure 5b). Although these images are only a qualitative demonstration, very few dead cells were visible after 48 h. This result clearly indicates the absence of cytotoxic impurities and provides strong experimental evidence for the excellent biocompatibility of the

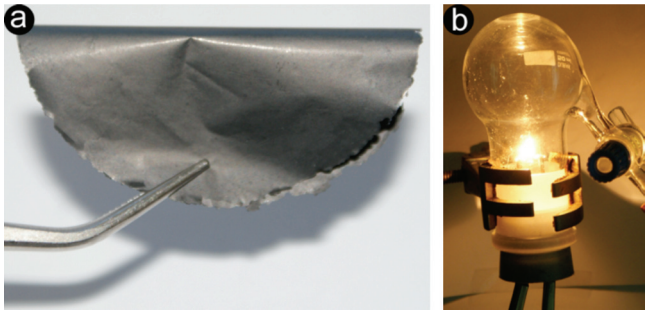

Figure 4. a) Highly flexible TRGO paper. b) "Graphene light bulb" operated at 19 V and 0.4 A in an argon atmosphere using TRGO paper as the glow filament.

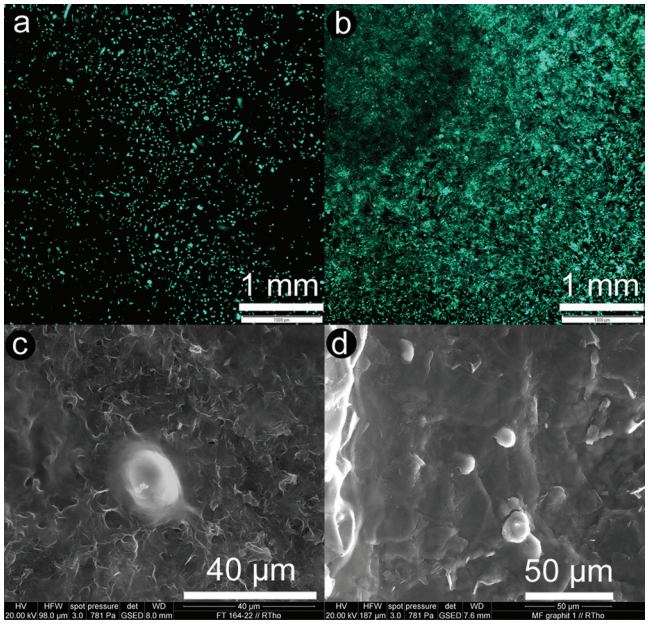

Figure 5. a,b) PI/FDA staining and c,d) ESEM images of human osteosarcoma cells (CAL 72) grown on TRGO paper (first column; a,c) and a pressed graphite tablet (second column; b,d). Green dots are living cells and dead cells would appear in red.

TRGO paper. However, compared with the graphite tablets, the cell population on the TRGO paper appears to be less dense. The environmental scanning electron microscopy (ESEM) images (Figure 5c,d) reveal that the TRGO paper surface is considerably rougher than that of the pressed graphite tablets. Whether this structural effect explains the reduced cell proliferation is the subject of ongoing studies.

2.3 Printing of Graphene Dispersions and Pastes

The direct printing of electrically conductive graphene inks using a commercial inkjet printer is a practical and low-cost method for the production of printed electronics. However, a homogenous graphene dispersion with a low viscosity (1–20 mPa s) and a matching surface tension is a key requirement for this printing process that prevents the clogging of the cartridge and enables the wetting and controlled coalescence of the microdroplets on the substrate.[20] Typically, ultrasonication and centrifugation cycles are needed for purification and fractionation.

At the Freiburg Materials Research Center (FMF), Mülhaupt and Landers developed a computer-guided printer based on a 3D microextrusion process, also known as 3D Bioplotting. Its applications are in the field of solid-free-form fabrication, rapid prototyping, and rapid manufacturing.[51,52] Although originally developed for scaffold fabrication and tissue engineering, this 3D printing technology is suitable for a variety of non-biological applications. The computer-guided 3D positioning of the nozzle, combined with a pneumatically controlled feed of melts, solutions, dispersions, and pastes, does not require piezoelectric valves or sonication. In contrast to commercial ink-jet printers,

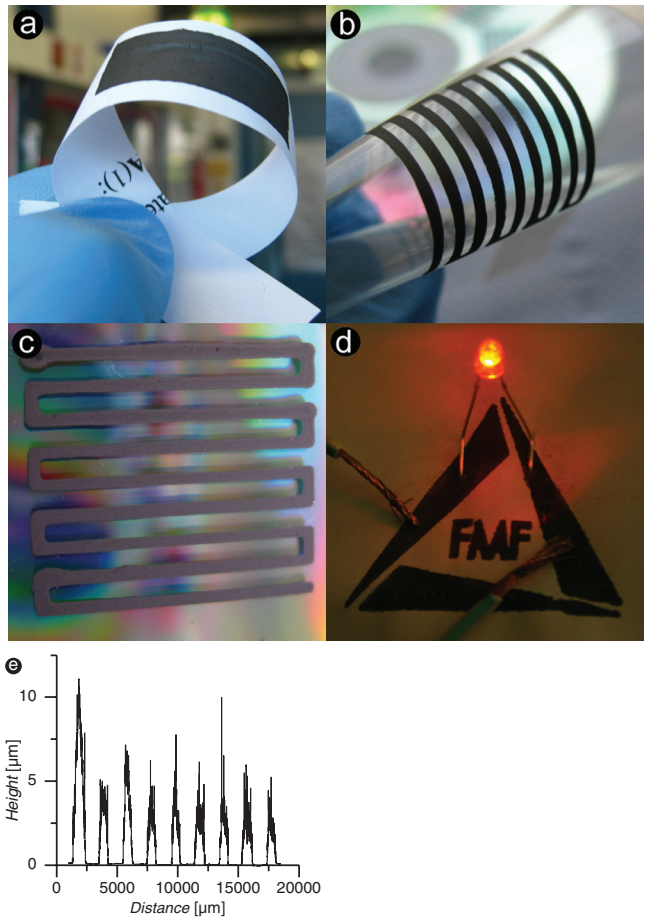

Figure 6. a–c) Printing TRGO on paper, PET-foil, and a CD, d) an electrically conductive printed FMF logo, and e) the height profile of the lines printed on a CD.

this printing method allows the processing of a wide range of materials with viscosities up to 1000 Pa s, including polymer melts and solutions, hydrogel precursors, polymer dispersions, and pastes of ceramics and metals.

For the first time, we have successfully employed this microextrusion-based 3D printing technique to process graphene pastes with high graphene content. Well-defined FG films were printed on a variety of materials, including paper (**Figure 6**a), inkjet printer foil (Figure 6b), and compact discs (CDs) (Figure 6c). In conventional inkjet printing, tiny droplets are deposited to fill out a given form. Because of surface tension, these droplets tend to merge, which can create gaps in the drawn film or line. This problem is avoided by the 3D microextrusion-based printing process because the lines are fabricated directly by microextrusion of the FG paste. Individually separated lines, line patterns and even dense or porous films of high uniformity and homogeneity can be printed using 3D microextrusion of FG dispersions. The FG dispersions solidify when the dispersion media vaporizes. Lines, layers and films with a thickness of up to 10 µm are formed in a single step (Figure 6d). In contrast, the conventional inkjet printing technique only leads to structures of approximately 300 nm and therefore requires repeated layer-by-layer printing.[23] To the best of our knowledge, this represents the first example of direct printing and 3D microextrusion of graphene pastes and dispersions with strong prospects for the large-scale manufacturing of novel graphene based materials and patterned surfaces.

Table 2. Comparisons of films produced by the direct printing of TRGO suspension, by the addition of a polymer binder and by the vacuum-assisted flow direction control.

Sample	Substrate	TRGO	TRGO content [g L^{-1}]	Binder (PVP) [g L^{-1}]	Film thickness [µm]	Electrical conductivity [S cm^{-1}]
printed film w/binder	paper	TRGO-900	20	1.2	17.0 ± 2.0	0.5 ± 0.2
printed film w/binder	foil	TRGO-900	20	1.2	6.0 ± 2.0	0.3 ± 0.1
printed film w/o binder	paper	TRGO-500	12.5	–	14.0 ± 2.0	8.3 ± 2.1
printed film w/o binder	foil	TRGO-500	12.5	–	5.0 ± 2.0	10.2 ± 3.6
flow-directed film	–	TRGO-400	0.3	–	9.0 ± 0.6	16.0 ± 1.0

To assess the electrical conductivity of TRGO films, elongated rectangles (30 × 10 mm^2) were printed on standard printing paper and inkjet printer foil in a standardized printing process. A binder-free TRGO dispersion (12.5 g L^{-1}) was used, and a TRGO dispersion (20 g L^{-1}) containing polyvinylpyrrolidone (PVP, 1.2 g L^{-1}) served as a reference for evaluating of the influence of a polymeric binder. The electrical conductivity of each printed film was determined using a four-point probe, and the geometry of the samples was taken into account with a correction factor.[53] The results shown in **Table 2** clearly demonstrate that the addition of even a small amount of binder strongly affects the electrical conductivity.

Although the concentration and degree of reduction of the TRGO are considerably higher in the samples containing a binder, the electrical conductivity is reduced by at least one order of magnitude when some binder is present. Thus, the ability to fabricate readily printable TRGO inks without the use of additives can be seen as an important step toward printed electronics. Compared to the conductivity of single flakes of TRGO (6.2–62 S cm^{-1}),[19] the values obtained are at the lower end of the conductivity range. Nevertheless, these values appear to be satisfactory because, in contrast to single flakes, the printed films contain a high number of sheet-to-sheet contacts. ESEM images of the printed films clearly illustrate the ragged structure of graphene sheets and the presence of flakes that lack a uniform orientation. When TRGO papers are produced by vacuum filtration, they have a tendency to assemble in a parallel flake alignment, which is probably caused by the flow direction (Figure SI. 2, Supporting Information). This result might explain the higher conductivities achieved by changing the flow direction.

Furthermore, these films have proven to be highly flexible, which allows them to bend and twist in almost any direction. In the field of printed electronics, the influence of mechanical stresses on the conductivity of the material is especially interesting. Other electrically conductive materials, such as indium

tin oxide (ITO) films, have proven to rapidly lose their conductivity when they are bent.[25] Because of this fact, bending experiments were performed on films printed on top of paper and foil. The films were used without further treatment and manually bent, first to the convex and then to the concave form. The sheet resistance was measured after every 100 bending cycles, and a total of 1000 bending cycles were performed. As shown in Figure SI.3 (Supporting Information), the electrical conductivity did not decrease significantly even after 1000 bending cycles.

3. Conclusions

The combination of thermal GO reduction followed by HPH is a versatile process for the clean and facile large-scale production of binder-, surfactant-, and nitrogen-free dispersions of functionalized graphene (FG) materials. When the high-surface-area TRGO suspension is forced through the narrow gap of the homogenizing valve at pressures of up to 1500 bar, high shear forces and turbulences account for the immediate TRGO fragmentation and lead to a very effective dispersion of the resulting single FG sheets in water, acetone, and isopropanol. In contrast to conventional CRGO-based FG dispersions, additional pre- and post-treatment steps and special dispersing agents are not required.

An essential feature of this HPH process is the presence of the oxygen-containing graphene functionality, e.g., hydroxyl, carboxyl and phenolic groups, which renders the FG amphiphilic. The oxygen content is readily controlled by varying the temperature of the thermal GO reduction. At an oxygen content above 10 wt%, coagulate-free stable aqueous dispersions are obtained without any purification. At lower oxygen content, graphene dispersions are readily obtained when large FG aggregates are removed via sedimentation. Only in the case of aqueous dispersions is the addition of small amounts of bases such as sodium hydroxide needed to enhance the dispersion of FG. The deprotonation of the carboxyl and hydroxyl groups potentially accounts for the in-situ formation of FG anions and the electrostatic FG stabilization by repulsion of the anionic FG sheets.

Non-aqueous FG dispersions are also produced by the HPH process even without addition of any bases. This enables the dispersion of FG in many other organic solvents, monomers, liquid rubbers, and thermoset resins by a simple exchange of the dispersion medium. Whereas many conventional approaches are limited to the formation of highly dilute graphene dispersions, the HPH process produces stable dispersions and pastes with an FG content between 0.01 and 15 g L^{-1}. These concentrated FG dispersions with high viscosity can be processed via a printing process based on microextrusion. During the printing process, the FG dispersions solidify upon the vaporization of the solvent and form micrometer-sized strands and layers. This microextrusion-based printing of FG pastes offers attractive opportunities for the fabrication of free-standing graphene films, graphene coatings, novel graphene hybrids, multilayer systems, gradient graphene layers, and micropatterned conductive graphene.

Applications for this technology range from packaging to engineering of lightweight materials, electromagnetic shielding and stealth technology, corrosion and abrasion protection, surface modification, electronics, microsystems engineering, and biomedicine. Moreover, in on-going research, highly viscous FG pastes are employed in 3D microextrusion and layer-by-layer printing of micropatterned surfaces and even larger 3D objects according to computer-assisted designs. This technique opens up a new avenue for the processing of carbon and hybrid carbon materials obtained by the blending of FG dispersions with other colloids and nanoparticles or by the immobilization of nanoparticles onto FG nanosheets. Because these films exhibit no observable cytotoxic behavior against human osteosarcoma cells, they are expected to be biocompatible. Patterns printed by microextrusion of graphene pastes have been proven to maintain their electrical conductivity even after excessive bending. Therefore, the combination of HPH and the computer-guided 2D and 3D microextrusion can be seen as a major step toward printed, highly flexible, carbon-based electronics and the fabrication of complex multilayer and gradient systems.

4. Experimental Section

Preparation of GO and TRGO: GO was prepared from a mixture of graphite (60 g, KFL99.5 Graphit Kropfmühl AG, Hauzenberg Germany), $NaNO_3$ (30 g, Merck KGaA, Darmstadt, Germany), $KMnO_4$ (180 g, Grüssing, Filsum Germany), and H_2SO_4 (95%, 1.4 L, VWR International GmbH, Darmstadt, Germany) according to Hummer's method.[9] The GO was rinsed several times in a Büchner funnel until no further SO_4^{2-} was detected by elemental analysis. After drying for 4 days at 40 °C under reduced pressure, the GO was ground up using a CryoMill (Retsch, Haan, Germany) and the resulting GO powder was dried for an additional 4 days. The dry GO powder was placed in a tube furnace with a N_2 atmosphere (Nabertherm, Lilienthal, Germany) and then heated at a specific reduction temperature (between 400 and 1000 °C) to yield TRGO powder. Elemental analysis was performed by combustion using a VarioEL-system (addition of WO_3, Elementaranalysesysteme, Hanau, Germany).

TRGO Suspensions: Aqueous TRGO suspensions were prepared by adding the as-prepared TRGO powder (0.3–15 g L^{-1}) to water and adjusting the pH to 9–10 by the addition of NaOH. In a typical procedure, a suspension (200 mL) was ultrasonicated for 10 min and then inserted into the high-pressure homogenizer (Panda NS1001, GEA Niro Soavi, Parma, Italy). Unless stated otherwise, a pressure of 1400 bar was applied during the homogenization to yield a graphene paste with TRGO concentrations of greater than 10 g L^{-1}, whereas lower concentrations resulted in less viscous suspensions. Suspensions in acetone or IPA were prepared in a similar manner, except without the addition of NaOH. TEM images of suspensions were obtained using a Zeiss/LEO 912 Ω transmission electron microscope (accelerating voltage 120kV, resolution 0.37 nm, Oberkochen, Germany).

Freestanding TRGO Papers: A TRGO suspension (0.3 g L^{-1}) was subjected to vacuum filtration using a polyester membrane (0.2 µm, 47 mm, Pieper Filter GmbH, Bad Zwischenahn, Germany) and subsequently rinsed with distilled water to remove NaOH impurities. After drying under ambient conditions overnight, followed by additional drying at 40 °C under vacuum, the TRGO papers were peeled off the filter.

Printing of Graphene Ink: The paste-like graphene ink was processed by the low-temperature head of the 3D-Bioplotter (3rd generation, Envisiontec, Gladbeck, Germany) (Figure SI. 4, Supporting Information). For conductivity measurements, rectangles (30×10 mm^2) were printed onto standard printer paper (80 g m^{-2}, m-real, Metsä, Finland) and inkjet printer foil (PET, Soennecken, Overath, Germany). The sheet resistance of all graphene films was measured using a four-point probe. A correction factor that depends on the sample geometry was taken into account in the calculations.[53]

Height Profile Measurement: Graphene patterns were printed on the bottom side of a CD (used for its very smooth surface). Height profile measurements were performed using a Dektat 150 surface profiler (Veeco, Plainview, NY, USA).

Biocompatibility Test: TRGO papers were prepared as described earlier in this paper. Graphite tablets were pressed using a standard tablet press. To remove the remaining residue, the samples were rinsed with Dulbecco's phosphate buffered saline (PBS) (without Ca^{2+} or Mg^{2+}, PAA Laboratories, Pasching, Austria) several times and subsequently sterilized (120 °C, 5 bar, 30 min) in an autoclave (model 3870 ELV, Tuttnauer, Breda, Netherlands) prior to use. Sterilized TRGO papers and graphite tablets (3× each) were placed in a 24-well plate (TCPS, Greiner, Frickenhausen, Germany), seeded with CAL 72 cells (human osteosarcoma cell line, ACC 439, German Collection of Microorganisms and Cell Cultures, DSMZ, Braunschweig, Germany) at a concentration of 1×10^5 per well and cultured in Dulbecco's modified Eagle medium (DMEM, Biowhittaker, Walkersville, MO, USA) with 10% fetal calf serum (FCS, PAA Laboratories, Pasching, Austria), 1% penicillin/streptomycin (Biochrom), and insulin transferrin (1 vial per 5 L medium) for 48 h in an incubator (Kendro-Heraeus). Cell viability was tested with a double staining procedure using fluorescein diacetate (FDA) and propidium iodide (PI) as specific fluorophores. Under a fluorescence microscope, viable cells appear green while dead cells are red. Images were obtained using a microscope (Axiover 135, Zeiss, Oberkochen, Germany) with a camera (AE 1, Canon). Prior to taking an ESEM image, samples were immersed in a formaldehyde solution to fix the cultivated cells (Quanta FEG 250, FEI, Eindhoven, Netherlands).

Supporting Information

Supporting Information is available from the Wiley Online Library or from the author.

Acknowledgements

F.J.T. and M.F. contributed equally to this work. The authors would like to thank BMBF (project 03X0111C, FUNgraphen) for funding the graphene synthesis. Additionally they would like to thank Ute Hübner for cell culture experiments and Dr. Ralf Thomann for TEM and SEM images.

Received: November 28, 2011
Published online: January 27, 2012

[1] H.-P. Boehm, R. Setton, B. Stumpp, *Pure Appl. Chem.* **1994**, *66*, 1893.
[2] A. A. Balandin, S. Ghosh, W. Bao, I. Calizo, D. Teweldebrhan, F. Miao, C. N. Lau, *Nano Lett.* **2008**, *8*, 902.
[3] C. Lee, X. Wei, J. W. Kysar, J. Hone, *Science* **2008**, *321*, 385.
[4] K. S. Novoselov, A. K. Geim, S. V. Morozov, D. Jiang, Y. Zhang, S. V. Dubonos, I. V. Crigorieva, A. A. Firsov, *Science* **2004**, *306*, 666.
[5] J. S. Bunch, S. S. Verbridge, J. S. Alden, A. M. van der Zande, J. M. Parpia, H. G. Craighead, P. L. McEuen, *Nano Lett.* **2008**, *8*, 2458.
[6] D. Li, M. B. Müller, S. Gilje, R. B. Kaner, G. G. Wallace, *Nat. Nanotechnol.* **2008**, *3*, 101.
[7] S. Park, J. An, R. D. Piner, I. Jung, D. Yang, A. Velamakanni, S. T. Nguyen, R. S. Ruoff, *Chem. Mater.* **2008**, *20*, 6592.
[8] H. Kim, A. A. Abdala, C. W. Macosko, *Macromolecules* **2010**, *43*, 6515.
[9] W. S. Hummers, R. E. Offeman, *J. Am. Chem. Soc.* **1958**, *80*, 1339.
[10] H.-P. Boehm, A. Clauss, G. O. Fischer, U. Hofmann, *Z. Naturforschg.* **1962**, *17 b*, 150.
[11] S. Stankovich, D. A. Dikin, R. D. Piner, K. A. Kohlhaas, A. Kleinhammes, Y. Jia, Y. Wu, S. T. Nguyen, R. S. Ruoff, *Carbon* **2007**, *45*, 1558.
[12] H. C. Schniepp, J.-L. Li, M. J. McAllister, H. Sai, M. Herrera-Alonso, D. H. Adamson, R. K. Prud´homme, R. Car, D. A. Saville, I. A. Aksay, *J. Phys. Chem. B* **2006**, *110*, 8535.
[13] M. J. McAllister, J.-L. Li, D. H. Adamson, H. C. Schniepp, A. A. Abdala, J. Liu, M. Herrera-Alonso, D. L. Milius, R. Car, R. K. Prud´homme, I. A. Aksay, *Chem. Mater.* **2007**, *19*, 4396.
[14] O. C. Compton, S. T. Nguyen, *Small* **2010**, *6*, 711.
[15] D. R. Dreyer, S. Park, C. W. Bielawski, R. S. Ruoff, *Chem. Soc. Rev.* **2010**, *39*, 228.
[16] S. Stankovich, R. D. Piner, X. Chen, N. Wu, S. T. Nguyen, R. S. Ruoff, *J. Mater. Chem.* **2006**, *16*, 155.
[17] K. Erickson, R. Erni, Z. Lee, N. Alem, W. Gannett, A. Zettl, *Adv. Mater.* **2010**, *22*, 4467.
[18] C. Gómez-Navarro, M. Burghard, K. Kern, *Nano Lett.* **2008**, *8*, 2045.
[19] T. Schwamb, B. R. Burg, N. C. Schirmer, D. Poulikakos, *Nanotechnology* **2009**, *20*, 405704.
[20] K.-Y. Shin, J.-Y. Hong, J. Jang, *Adv. Mater.* **2011**, *23*, 2113.
[21] L. T. Le, M. H. Ervin, H. Qiu, B. E. Fuchs, W. Y. Lee, *Electrochem. Commun.* **2011**, *13*, 355.
[22] S. Wang, P. K. Ang, Z. Wang, A. L. L. Tang, J. T. L. Thong, K. P. Loh, *Nano Lett.* **2010**, *10*, 92.
[23] J. M. Crain, J. S. Lettow, I. A. Aksay, S. Korkut, K. S. Chiang, C. Chen, R. K. Prud'homme, *World Patent WO002009099707A1***2009**.
[24] V. Dua, S. Surwade, S. Ammu, S. Agnihotra, S. Jain, K. Roberts, S. Park, R. Ruoff, S. Manohar, *Angew. Chem. Int. Ed.* **2010**, *49*, 2154.
[25] H. Chang, G. Wang, A. Yang, X. Tao, X. Liu, Y. Shen, Z. Zheng, *Adv. Funct. Mater.* **2010**, *20*, 2893.
[26] M. Lotya, P. J. King, U. Khan, S. De, J. N. Coleman, *ACS Nano* **2010**, *4*, 3155.
[27] Y. Si, E. T. Samulski, *Nano Lett.* **2008**, *8*, 1679.
[28] S. Stankovich, D. A. Dikin, G. H. B. Dommett, K. M. Kohlhaas, E. J. Zimney, E. A. Stach, R. D. Piner, S. T. Nguyen, R. S. Ruoff, *Nature* **2006**, *442*, 282.
[29] S. Stankovich, R. D. Piner, S. T. Nguyen, R. S. Ruoff, *Carbon* **2006**, *44*, 3342.
[30] Z. Lin, Y. Liu, C.-p. Wong, *Langmuir* **2010**, *26*, 16110.
[31] A. B. Bourlinos, D. Gournis, D. Petridis, T. Szabó, A. Szeri, I. Dékány, *Langmuir* **2003**, *19*, 6050.
[32] M. J. Fernández-Merino, L. Guardia, J. I. Paredes, S. Villar-Rodil, P. Solís-Fernández, A. Martínez-Alonso, J. M. D. Tascón, *J. Phys. Chem. C.* **2010**, *114*, 6426.
[33] A. Abouimrane, O. C. Compton, K. Amine, S. T. Nguyen, *J. Phys. Chem. C.* **2010**, *114*, 12800.
[34] C. Wang, D. Li, C. O. Too, G. G. Wallace, *Chem. Mater.* **2009**, *21*, 2604.
[35] D. A. Dikin, S. Stankovich, E. J. Zimney, R. D. Piner, G. H. B. Dommett, G. Evmenenko, S. T. Nguyen, R. S. Ruoff, *Nature* **2007**, *448*, 457.
[36] S. H. Lee, H. W. Kim, J. O. Hwang, W. J. Lee, J. Kwon, C. W. Bielawski, R. S. Ruoff, S. O. Kim, *Angew. Chem. Int. Ed.* **2010**, *49*, 10084.
[37] H. Chen, M. B. Müller, K. J. Gilmore, G. G. Wallace, D. Li, *Adv. Mater.* **2008**, *20*, 3557.
[38] I. K. Moon, J. Lee, R. S. Ruoff, H. Lee, *Nat. Commun.* **2010**, *1*, 73.
[39] F. Liu, T. S. Seo, *Adv. Funct. Mater.* **2010**, *20*, 1930.
[40] Q. Zhang, Y. Qiao, F. Hao, L. Zhang, S. Wu, Y. Li, J. Li, X.-M. Song, *Chem. Eur. J.* **2010**, *16*, 8133.
[41] K. Liu, J.-J. Zhang, F.-F. Cheng, T.-T. Zheng, C. Wang, J.-J. Zhu, *J. Mater. Chem.* **2011**, *21*, 12034.
[42] S. Y. Park, J. Park, S. H. Sim, M. G. Sung, K. S. Kim, B. H. Hong, S. Hong, *Adv. Mater.* **2011**, *23*, H263.
[43] M. Kalbacova, A. Broz, J. Kong, M. Kalbac, *Carbon* **2010**, *48*, 4323.

[44] K. Yang, S. Zhang, G. Zhang, X. Sun, S.-T. Lee, Z. Liu, *Nano Lett.* **2010**, *10*, 3318.
[45] N. Li, X. Zhang, Q. Song, R. Su, Q. Zhang, T. Kong, L. Liu, G. Jin, M. Tang, G. Cheng, *Biomaterials* **2011**, *32*, 9374.
[46] Vorbeck Materials, http://www.vorbeck.com/(accessed January 2012).
[47] A. Radoi A. Iordanescu, A. Cismaru, M. Dragoman, D. Dragoman, *Nanotechnology* **2010**, *21*, 455202.
[48] NanoIntegris, http://www.nanointegris.com/en/puresheets (accessed January 2010).
[49] F. Li, Y. Bao, J. Chai, Q. Zhang, D. Han, L. Niu, *Langmuir* **2010**, *26*, 12314.
[50] U. Hofmann, A. Frenzel, E. Csalán, *Justus Liebigs Ann. Chem.* **1934**, *510*, 1.
[51] R. Landers, A. Pfister, U. Hübner, H. John, R. Schmelzeisen, R. Mülhaupt, *J. Mater. Sci.* **2002**, *37*, 3107.
[52] R. Landers, U. Hübner, R. Schmelzeisen, R. Mülhaupt, *Biomaterials* **2002**, *23*, 4437.
[53] S. M. Sze, *Physics of semiconductor devices*, 2nd Ed., Wiley-Interscience, New York **1982** .